Particuology xxx (2014) xxx–xxx

Contents lists available at ScienceDirect

Particuology

journal homepage: www.elsevier.com/locate/partic

Invited paper

Effects of cerium incorporation on the catalytic oxidation of benzene over flame-made perovskite $La_{1-x}Ce_xMnO_3$ catalysts

Gang Liu[a,b], Jiaqi Li[a,b], Kun Yang[a], Wenxiang Tang[a,b], Haidi Liu[a], Jun Yang[a], Renliang Yue[a,**], Yunfa Chen[a,*]

[a] State Key Laboratory of Multi-phase Complex Systems, Institute of Process Engineering, Chinese Academy of Sciences, Beijing 100190, China
[b] University of Chinese Academy of Sciences, Beijing 100049, China

ARTICLE INFO

Article history:
Received 3 March 2014
Received in revised form 29 April 2014
Accepted 10 July 2014

Keywords:
Perovskite
Benzene elimination
Ce substitution
Flame spray pyrolysis
Charge neutralization

ABSTRACT

Perovskite-type $La_{1-x}Ce_xMnO_3$ (x = 0–10%) catalysts were prepared by flame spray pyrolysis and their activities during the catalytic oxidation of benzene were examined over the temperature range of 100–450 °C. The structural properties and reducibility of these materials were also characterized by X-ray diffraction (XRD), N_2 adsorption/desorption, H_2 temperature-programmed reduction (H_2-TPR) and X-ray photoelectron spectroscopy (XPS). The incorporation of Ce was found to improve the benzene oxidation activity, and the perovskite in which x was 0.1 exhibited the highest activity. Phase composition and surface elemental analyses indicated that non-stoichiometric compounds were present. The incorporation of Ce had a negligible effect on the specific surface area of the perovskites and hence this factor has little impact on the catalytic activity. Introduction of Ce^{4+} resulted in modification of the chemical states of both B-site ions and oxygen species and facilitated the reducibility of the perovskite. The surface Mn^{4+}/Mn^{3+} ratio was increased as a result of Ce^{4+} substitution, while a decrease in the surface-adsorbed O/lattice O (O_{ads}/O_{latt}) ratio was observed. The relationship between the surface elemental ratios and catalytic activity was established to allow a better understanding of the process by which benzene is oxidized over perovskites.

Introduction

Perovskite-structure oxides (ABO_3) are receiving significant attention in the field of catalysis, especially with regard to the catalytic oxidation of volatile organic compounds (VOCs), based on their exceptional catalytic activity and thermal stability (Pecchi, Reyes, Zamora, Cadus, & Fierro, 2008; Royer, Alamdari, Duprez, & Kaliaguine, 2005; Wen, Zhang, He, Yu, & Teraoka, 2007). To date, ABO_3 perovskites have been applied to the catalytic flameless combustion of methane (Buchneva et al., 2009; Campagnoli et al., 2005; Rossetti, Biffi, & Forni, 2010), the oxidation of ethanol (Najjar & Batis, 2010), the selective catalytic reduction of NO_x (Chiarello, Ferri, Grunwaldt, Forni, & Baiker, 2007), the removal of diesel soot particulates (Teraoka, Kanada, & Kagawa, 2001), and the catalytic removal of ethyl acetate (Niu et al., 2007), acetone (Spinicci, Faticanti, Marini, De Rossi, & Porta, 2003), isopropanol and benzene (Blasin-Aube, Belkouch, & Monceaux, 2003). Within this series of perovskites, $LaMnO_3$ exhibits superior properties and catalytic performance (Li, Wang, & Gong, 2009), and this may be attributed to the inherent high specific surface area (SSA) of this material, the presence of a stoichiometric excess of oxygen, a defective/cation-deficient lattice, and the presence of manganese in multiple oxidation states (Mn^{3+}/Mn^{4+}). These properties can be further enhanced by the doping of certain metal oxide species, such as Ce ions, into the $LaMnO_3$ structure, such that La ions are partly substituted by the dopant ions (Kaddouri, Gelin, & Dupont, 2009).

Ceria in its natural form is a poor catalyst. However, the activity of certain catalysts can be dramatically improved by the incorporation of Ce (Zhang-Steenwinkel, Beckers, & Bliek, 2002). Oxygen storage capacity (OSC) is a characteristic property of Ce^{3+}/Ce^{4+} ions and the synergistic effect between Ce^{3+}/Ce^{4+} and Mn^{3+}/Mn^{4+} has been shown to enhance catalytic activity (Royer et al., 2005).

* Corresponding author. Tel.: +86 10 82627057; fax: +86 10 82544919.
** Corresponding author. Tel.: +86 10 82544895; fax: +86 10 82544919.
E-mail addresses: rlyue@ipe.ac.cn (R. Yue), yfchen@ipe.ac.cn (Y. Chen).

http://dx.doi.org/10.1016/j.partic.2014.07.001
1674-2001/

Extensive studies have examined the substitution of Ce into catalytic materials and the influence of the preparation method applied. Alifanti, Kirchnerova, and Delmon (2003) studied the effects of Ce incorporation on $La_{1-x}Ce_xMnO_3$ ($x = 0.1$, 0.2, 0.3, 0.4, and 0.5) catalysts, focusing on the relationship between physicochemical properties and catalytic activity. These catalysts were obtained by the citrate method and the study employed the combustion of 1% methane in air as a model catalytic reaction. It was determined that the substitution of cerium at the level of $x = 0.1$ had beneficial effects, whereas higher x values resulted in lower catalytic activity and higher cost. Kaddouri et al. (2009) reported the relationship between the physicochemical properties and catalytic performance of La–Ce–Mn–O perovskites obtained by different preparation methods. Samples prepared by the conventional hydrothermal and dielectric heating hydrothermal methods were tested for methane combustion. Higher CH_4 conversion and better sulfur tolerance were exhibited by the samples synthesized by the dielectric heating hydrothermal method. The superior catalytic performance was attributed to good dispersion of the various cerium oxide species as well as strong interactions between these cerium species and the $LaMnO_3$ host structure.

A catalyst that combines high surface area, high ionic mobility through the crystal lattice, and the potential for large-scale production is difficult to obtain by traditional methods. Recently, flame spray pyrolysis (FSP) was developed as a means of synthesizing various different kinds of metal oxides, either in lab-scale or large-scale quantities (Chiarello, Rossetti, & Forni, 2005; Chiarello, Rossetti, Lopinto, Migliavacca, & Forni, 2006). In general, FSP is a versatile, convenient, and cost-effective process for the production of ceramic nanoparticles. In a typical flame spray pyrolysis setup, a liquid precursor including a high or low combustion enthalpy solvent is aerosolized by a dispersion gas (oxygen or air) as it passes through a spray nozzle, and subsequently combusts in a support flame in the vicinity of the spray nozzle. The flame temperature in this process is thought to exceed 1000 °C in the main flame zone depending on the gas flow rate, the liquid precursor feed rate, the setup parameters, and the nature of the solvent (Liu, Yue, et al., 2013). Chiarello et al. (2005) reported the synthesis of nano-sized $LaCoO_3$ and its application to the catalytic combustion of methane. The effect of the solvent on the preparation of perovskites by FSP was also studied. In this work, Pd particles were systematically introduced into the $LaCoO_3$ simply by adding an appropriate metal precursor to the liquid precursor. Further studies on the catalytic performance during the reduction of NO by H_2 under lean-burn conditions have also been performed (Chiarello, Ferri, et al., 2007; Chiarello, Grunwaldt, et al., 2007). Additional structures, such as $MgAl_2O_4$ spinel (Roy, van Vegten, & Baiker, 2010), a $NiO–Al_2O_3$ core–shell structure (Azurdia et al., 2006) and a noble metal-loaded Pt/TiO_2 (Teoh, Madler, Beydoun, Pratsinis, & Amal, 2005), have been obtained by FSP or by variants of FSP.

Nano-sized catalysts formed by flame spray pyrolysis are characterized by high specific surface areas and high ionic mobility through the crystal lattice and they are also highly crystalline. In the present study, $LaMnO_3$ substituted with Ce was synthesized as a model catalyst to investigate the inherent relationships between structure, surface element composition, reducibility, and catalytic activity. Various characterization methods, such as Transmission Electron Microscopy (TEM), XRD, XPS, and H_2-TPR, were used to examine the nature of these flame-made catalysts. This study focused in particular on the physicochemical properties of the $La_{1-x}Ce_xMnO_3$ perovskites synthesized by flame spray pyrolysis and the catalytic performances of these materials for the complete oxidation of benzene.

Experimental

Materials

Propanoic acid (CP), lanthanum acetate (99.99%), cerium acetate (99.99%) and manganese acetate (99.9%) were purchased from the Sinopharm Company and used as received without any further purification.

Catalyst preparation

$La(CH_3COO)_3{\cdot}6H_2O$, $Ce(CH_3COO)_3{\cdot}6H_2O$, and $Mn(CH_3COO)_2{\cdot}4H_2O$ were used as La, Ce, and Mn sources, respectively. Liquid precursors with a La to Mn molar ratio of 1:1 were obtained by dissolving the appropriate quantities of the corresponding metal precursors in propanoic acid, during which time the liquid precursor was stirred at 1200 rpm at 70 °C for 20 min. Stoichiometric $Ce(CH_3COO)_3{\cdot}6H_2O$ was subsequently mixed into the liquid precursor. The total metal (La + Mn) concentration of the liquid precursor was 0.2 M when preparing the $La_{1-x}Ce_xMnO_3$ perovskites (where x represents the nominal mole fraction of Ce incorporated into the perovskite structure, $x = 0$, 2.5%, 5.0%, 7.5%, and 10.0%).

Perovskite-structure catalysts were synthesized by FSP, using a process described elsewhere in detail (Liu, Yue, et al., 2013). In brief, the liquid precursor was supplied by a peristaltic pump and sprayed through a nozzle in a stream of oxygen. The precursor supply rate and the dispersion oxygen flow rate were set to 10.27 mL/min and 4.0 L/min, respectively. The sprayed precursor was ignited by a support flame derived from a combination of oxygen and methane with flow rates of 4.0 and 2.4 L/min, respectively. The resulting particles were collected on a glass fiber filter with the aid of a vacuum pump. On average, approximately 6.6 g of powder was collected on the filter per hour during operation of the lab-scale FSP apparatus. During FSP, a yellow-green flame was observed for all the samples, whereas the as-prepared powders exhibited a black coloration.

Catalyst characterization

Data concerning the phases of the $La_{1-x}Ce_xMnO_3$ perovskites were obtained by X-ray diffractometer (XRD, X'Pert Pro), applying scans from 5° to 90° (2θ) with Cu Kα ($\lambda = 1.54$ Å) radiation. Phases were identified by comparison with JCPD 51-1516 (lanthanum manganese oxide). The average crystallite sizes and cell parameters were calculated using the Scherrer equation. Specific surface areas were determined by employing the BET method, using data from an Autosorb-1-C-TCD (Quantachrome Instruments). Prior to measurements, powder samples (ca. 200 mg) were pretreated at 300 °C for 3 h to remove moisture. A JSM-6700F field emission scanning electron microscope (FESEM) and a JEM 2100F electron microscope (JEOL, Japan) combined with X-ray energy dispersive spectroscopy (EDX) were used to characterize the morphology of the $La_{1-x}Ce_xMnO_3$ perovskites. XPS data were obtained with an ESCALab220i-XL electron spectrometer (VG Scientific, UK) using 300 W Al Kα radiation. The base pressure during these measurements was approximately 3×10^{-9} mbar. The binding energies were referenced to the C 1s line at 284.8 eV from adventitious carbon. H_2-TPR was performed on a Micromeritics Chemisorb 2720 pulse chemisorption system (Micromeritics, USA) equipped with a TPx system and a thermal conductivity detector (TCD). Samples of approximately 30 mg were heated from ambient temperature to 850 °C at 10 °C/min and a mixture of H_2 (10 vol%) and Ar was employed as a reducing atmosphere at a flow rate of 25 mL/min.

Please cite this article in press as: Liu, G., et al. Effects of cerium incorporation on the catalytic oxidation of benzene over flame-made perovskite $La_{1-x}Ce_xMnO_3$ catalysts. *Particuology* (2014), http://dx.doi.org/10.1016/j.partic.2014.07.001

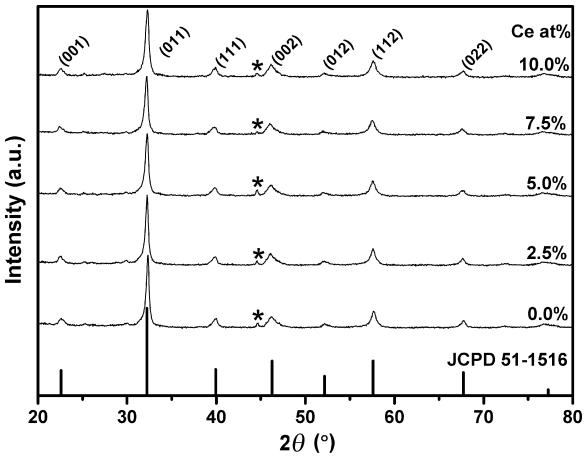

Fig. 1. XRD patterns of $La_{1-x}Ce_xMnO_3$ ($x = 0$, 2.5%, 5.0%, 7.5%, and 10.0%) catalysts synthesized by flame spray pyrolysis.

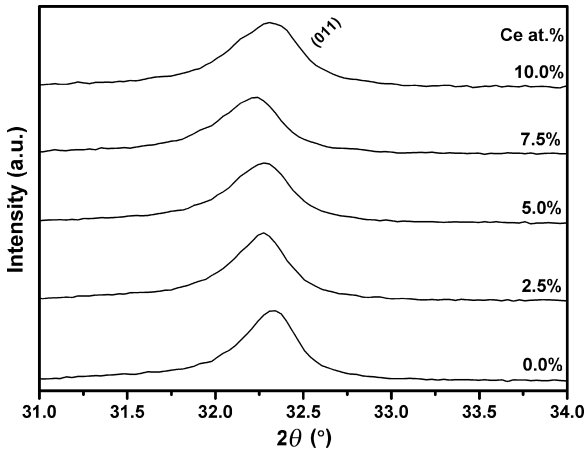

Fig. 2. Details of the characteristic peak of the $La_{1-x}Ce_xMnO_3$ perovskites ($x = 0$, 2.5%, 5.0%, 7.5%, and 10.0%), highlighting the shift and broadening of the peak corresponding to the (0 1 1) crystal plane.

Catalytic activity measurements

Measurements of the catalytic reaction of benzene were performed in an atmospheric fixed bed reactor, heated from 100 to 450 °C. Catalyst samples of approximately 100 mg (40–60 mesh) were transferred into a quartz tube reactor (i.d. = 6 mm) and enclosed on both sides with two layers of silica wool. N_2 gas containing 1000 ppm benzene was mixed with O_2 to generate a total flow rate of 100 mL/min, corresponding to a weight hourly space velocity (WHSV) of 60,000 mL/(g h). Exhaust gas exiting the reactor was analyzed by a gas chromatograph (GC, Agilent, 6890N, USA) equipped with a flame ionization detector (FID). The total conversion of benzene, $X_{benzene}$ (%), was calculated using the following equation

$$X_{benzene}\ (\%) = \frac{[benzene]_{In} - [benzene]_{Out}}{[benzene]_{In}} \times 100,$$

where $[benzene]_{In}$ and $[benzene]_{Out}$ are the concentrations of benzene in the inlet gas and outlet gas, respectively.

Results and discussion

Crystal phase, morphology, and surface area

Fig. 1 shows the XRD patterns of fresh $La_{1-x}Ce_xMnO_3$ ($x = 0$, 2.5%, 5.0%, 7.5%, and 10.0%) catalysts synthesized by flame spray pyrolysis. The pattern of the pure perovskite $LaMnO_3$ ($x = 0$) is consistent with that of JCPD 51-1516, which corresponds to lanthanum manganese oxide. The main phase corresponds to $La_{1-x}Mn_{1-z}O_3$ (non-stoichiometric) and the weak peaks labeled with asterisks in the figure may be assigned to MnO_x species that have appeared because of non-stoichiometry. The presence of small amounts of MnO_x species is in agreement with the results of earlier studies (Asamoto and Yahiro, 2009).

The patterns obtained for the $La_{1-x}Ce_xMnO_3$ perovskites are provided in Fig. 1, ranked according to increasing Ce concentration, along with that of pure perovskite $LaMnO_3$. The intensity of the peaks indicates highly crystalline structures, as observed in the TEM images, in which a distinct lattice structure can be distinguished. Based on these peaks, a CeO_2 phase was absent in the perovskite catalysts, which suggests that La^{3+} was partially substituted by Ce in the perovskite structure, especially at high Ce concentrations (Zhang-Steenwinkel et al., 2002). The absence of lines corresponding to a CeO_2 phase suggests that the point of saturation with regard to cerium substitution was not reached at $x = 0.1$, while a CeO_2 phase was obviously present at a degree of substitution above 0.2 (Zhang-Steenwinkel et al., 2002). The peaks assigned to the (0 1 1) crystal planes (around 32.3°) are the main feature of the perovskite lattice structure, and both shifting and broadening of the (0 1 1) peaks can be observed with increasing Ce concentrations, as shown in detail in Fig. 2.

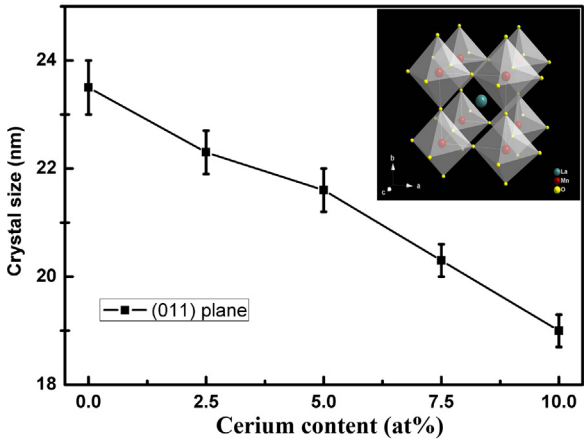

Fig. 3. Crystal size constraint effects in $La_{1-x}Ce_xMnO_3$ perovskites. Crystal sizes were calculated from the FWHM of peaks corresponding to the (0 1 1) plane, using the Scherrer equation.

Detailed information concerning the variations of the characteristic peak of the $LaMnO_3$ perovskite structure with differing Ce concentrations is presented in Fig. 2. It is evident that the (0 1 1) peaks broaden with increasing Ce concentrations and that the 2θ value also shifts to smaller angles. These results indicate that increased Ce concentration leads to broadening and peak shifts in the XRD pattern due to changes or distortions of the cell lattice. According to the Scherrer equation, broader peaks reflect smaller crystal sizes, as illustrated in detail in Fig. 3, which plots the crystal sizes calculated from broadening the peaks corresponding to the (0 1 1) crystal plane. As shown in the figure, the crystal size tended to decrease linearly with increases in the Ce concentration.

The inset in Fig. 3 shows the structure of a conventional $LaMnO_3$ perovskite as derived from XRD data. $LaMnO_3$ crystallizes in two well-determined phases at ambient temperature: orthorhombic and rhombohedric (Talati and Jha, 2006). A structural phase transition occurs at approximately 750 K and cubic perovskites are present at ambient pressure (Pinsard-Gaudart et al., 2001). The

Please cite this article in press as: Liu, G., et al. Effects of cerium incorporation on the catalytic oxidation of benzene over flame-made perovskite $La_{1-x}Ce_xMnO_3$ catalysts. *Particuology* (2014), http://dx.doi.org/10.1016/j.partic.2014.07.001

Table 1
Physical and chemical properties of $La_{1-x}Ce_xMnO_3$ perovskites (x = 0, 2.5%, 5.0%, 7.5%, and 10.0%).

Catalysts	d_{XRD} (nm)[a]	$d_{(0\,1\,1)}$ (Å)[a]	SSA (m^2/g)
$LaMnO_3$	23.5 (0.5)	2.7661 (0.0004)	27.20
$La_{0.975}Ce_{0.025}MnO_3$	22.3 (0.4)	2.7711 (0.0004)	24.05
$La_{0.950}Ce_{0.050}MnO_3$	21.6 (0.4)	2.7715 (0.0005)	24.98
$La_{0.925}Ce_{0.075}MnO_3$	20.3 (0.3)	2.7764 (0.0005)	27.32
$La_{0.900}Ce_{0.100}MnO_3$	19.0 (0.3)	2.7681 (0.0006)	25.38

[a] d_{XRD} and $d_{(0\,1\,1)}$ are calculated according to (0 1 1) peak of XRD diffraction.

synthesis method and conditions have a significant impact on the phase formation and the cubic perovskites present in this study can be attributed to the nature of FSP. In the flame zone, precursor droplets experience rapid combustion and quenching within a few milliseconds, at a temperature reported to exceed 1000 °C (Thiebaut, 2011). This temperature and the attendant extreme conditions are not present in the traditional method and thus a structural phase transition to cubic phase perovskite may be assumed in FSP.

In the flame-made $La_{1-x}Ce_xMnO_3$ catalysts, Ce^{4+} partially substitutes for La^{3+}, as is often the case in other perovskites (Wen et al., 2007). The cerium concentration in the resulting perovskite structure affects the surrounding lattice because of changes in both ion size and valency (or degree of coordination), since the ionic radius of Ce^{4+} (0.92 Å) is smaller than that of La^{3+} (1.17 Å). Dopant size is reported to increase the d spacing of the (0 1 1) crystal plane, which subsequently generates a peak shift to a smaller angle in the XRD pattern according to the Scherrer equation. Therefore, the partial substitution of La by Ce at the A-site of the perovskite should lead to shrinkage of the unit cell and hence the crystal size. Ionic valency or degree of coordination has an impact on the surrounding lattice. In the $La_{1-x}Ce_xMnO_3$ perovskite structure, the higher valency of Ce^{4+} should result in greater coordination with surrounding O compared with that of La^{3+} within the same crystal plane, which would hinder the crystal growth and ultimately lead to a smaller crystal size. The crystal size constraint effects of both size and valency are demonstrated in the decreased crystal sizes in the (0 1 1) plane as the Ce concentration is increased. According to the (0 1 1) peak data obtained from XRD diffraction, a linear decrease in the crystallite size from 23.5 nm for $LaMnO_3$ to 19.0 nm for $La_{0.900}Ce_{0.100}MnO_3$ is observed, as shown in Fig. 3.

All the $La_{1-x}Ce_xMnO_3$ catalysts exhibited moderate specific surface areas (24.05–27.32 m^2/g, Table 1), which is characteristic of perovskite materials synthesized by FSP. This indicates that the addition of cerium to $LaMnO_3$ seems to have had little impact on the specific surface areas of these catalysts.

TEM images of pure $LaMnO_3$ and the $La_{0.900}Ce_{0.100}MnO_3$ perovskite are provided in Fig. 4. In the case of the pure $LaMnO_3$ perovskite, particles with average diameters less than 40 nm are seen throughout the images and these particles exhibit multi-faceted morphology at high magnification. In the HRTEM images, the distinct crystal lattice indicates highly crystallized particles, which is consistent with XRD results. The d spacing of the (0 1 1) plane obtained from these images is 2.76 Å, which confirms the phase information and is consistent with the spacing of 2.76 Å for the (0 1 1) plane in JCPD 51-1516. Corresponding EDX results are shown below, in Fig. 4(e), and demonstrate the absence of impurities in the selected area. Cu and C peaks in this pattern may be attributed to the presence of a standard Cu grid covered by carbon film. The mole percentages of La and Mn are 11.0% and 10.49%, indicating the formation of stoichiometric $LaMnO_3$. With regard to the $La_{0.900}Ce_{0.100}MnO_3$ perovskite, the TEM images are very similar to those of the pure $LaMnO_3$, showing particles with average diameters less than 40 nm. The multi-faceted particles coupled with

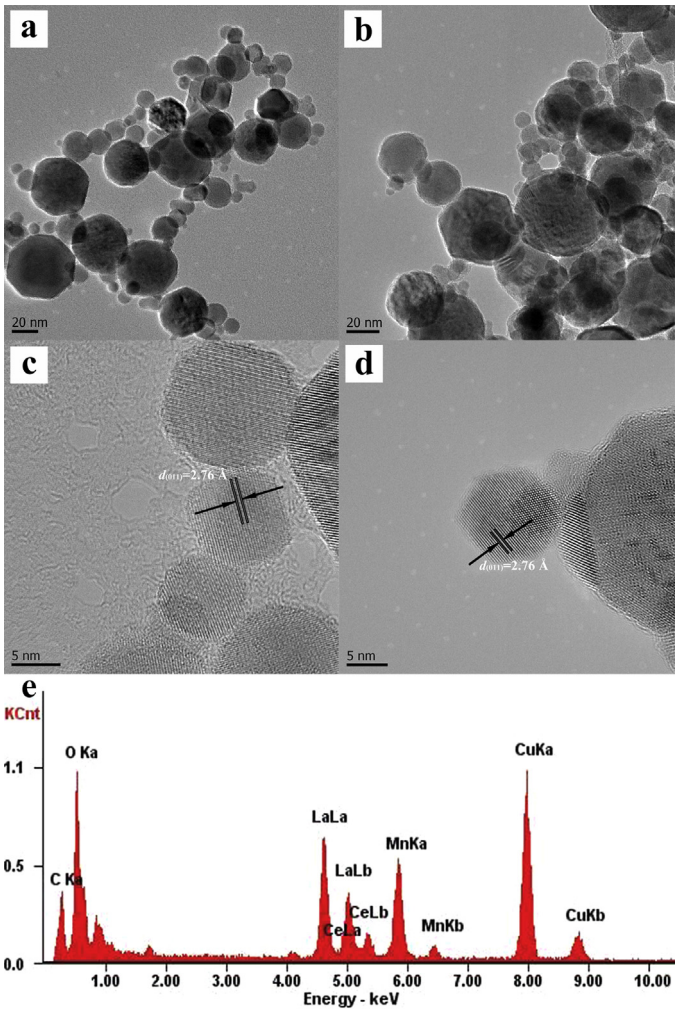

Fig. 4. TEM images of (a) pure $LaMnO_3$ and (b) $La_{0.900}Ce_{0.100}MnO_3$ perovskites; HRTEM images of (c) pure $LaMnO_3$ and (d) $La_{0.900}Ce_{0.100}MnO_3$ perovskites; and (e): a corresponding EDX image of (e) $La_{0.900}Ce_{0.100}MnO_3$ perovskites.

clearly defined crystal lattice images suggest a high degree of crystallinity. The d spacing of the (0 1 1) plane obtained from the HRTEM images is again 2.76 Å, thus there is no significant change between $LaMnO_3$ and the $La_{0.900}Ce_{0.100}MnO_3$ perovskite. The SEM images of $LaMnO_3$ and $La_{1-x}Ce_xMnO_3$ (x = 7.5%) are provided in Fig. S1.

Surface composition, metal oxidation and oxygen species

Fig. 5 shows the Mn 2p and O1s XPS spectra of the $La_{1-x}Ce_xMnO_3$ (x = 0, 2.5%, 5.0%, 7.5%, and 10.0%) catalysts. It can be seen from Fig. 5(a) that the peaks corresponding to Mn 2p3/2 and Mn 2p5/2 are broad and asymmetric toward the high binding energy side. The binding energies of C 1s, O 1s, and Mn 2p3/2 core-levels are summarized in Table 2. To obtain the identities of the Mn species, the Mn 2p3/2 and Mn 2p5/2 peaks of each sample were broken down into three components corresponding to binding energies of 614.4, 642.8, and 644.7 eV. These three components can be assigned to surface Mn^{3+} and Mn^{4+} species and to the satellite of Mn^{3+} species, respectively. According to Kucharczyk and Tylus (2008), the absence of a satellite peak at +5 eV from the Mn 2p3/2 peak suggests that no Mn^{2+} is present. Moreover, the presence of the two Mn species (Mn^{4+} and Mn^{3+}) is also indicated by the H_2-consumption peaks in the H_2-TPR data (discussed later). As summarized in Table 2, a relationship between the surface Mn^{4+}/Mn^{3+} ratio and

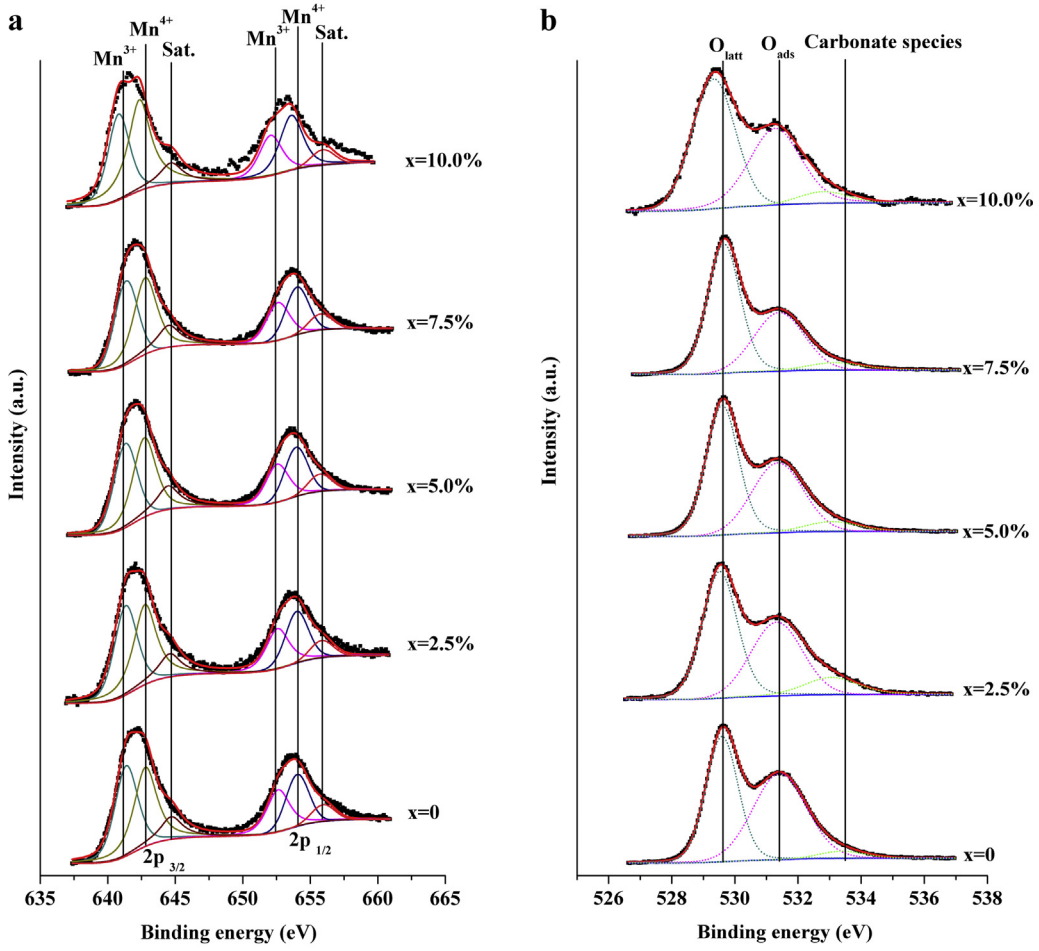

Fig. 5. XPS spectra of $La_{1-x}Ce_xMnO_3$ (x = 0, 2.5%, 5.0%, 7.5%, and 10.0%) catalysts. (a) Mn 2p and (b) O 1s.

the Ce concentration is observed, such that the ratio increases from 1.01 for $LaMnO_3$ to 1.40 for $La_{0.900}Ce_{0.100}MnO_3$.

For each sample, the O 1s spectrum in Fig. 5(b) can also be broken down into three components with binding energies of 529.6, 531.4, and 533.4 eV. The low binding energy at 529.6 eV is generally accepted as the result of surface lattice oxygen (O_{latt}: O^{2-}), while 531.4 eV can be assigned to adsorbed oxygen (O_{ads}: O^-, O_2^-, or O_2^{2-}) and 533.4 eV is due to carbonate species. The surface O_{ads}/O_{latt} ratio evidently decreases dramatically after the addition of cerium to the perovskite catalysts (Ponce, Peña, & Fierro, 2000). As can be seen from Table 2, the surface O_{ads}/O_{latt} ratio is 1.11 for $LaMnO_3$ and less than 1 for $La_{1-x}Ce_xMnO_3$ (x = 2.5%, 5.0%, 7.5%, and

Table 2
Surface elemental compositions and catalytic activities of $La_{1-x}Ce_xMnO_3$ perovskites (x = 0, 2.5%, 5.0%, 7.5%, and 10.0%).

x (%)	C 1s	O 1s	Mn 2p	Surface Mn^{4+}/Mn^{3+} ratio	Surface O_{ads}/O_{latt} ratio	Benzene oxidation activity		
						T_{10} (°C)	T_{50} (°C)	T_{90} (°C)
0	284.8 (51.0)[a] 286.3 (26.8) 289.4 (22.2)	529.6 (45.7) 531.4 (50.8) 533.4 (3.5)	641.4 (43.0) 642.8 (43.3) 644.7 (13.7)	1.01	1.11	258	340	>450
2.5	284.8 (71.5) 286.2 (13.5) 288.9 (15.0)	529.5 (50.0) 531.3 (39.2) 533.0 (10.8)	641.3 (41.4) 642.8 (44.7) 644.6 (13.9)	1.08	0.78	253	320	434
5.0	284.8 (58.7) 286.4 (20.6) 289.2 (20.7)	529.6 (52.8) 531.4 (41.0) 533.0 (6.2)	641.3 (40.0) 642.7 (44.3) 644.5 (15.7)	1.11	0.78	253	323	450
7.5	284.8 (57.3) 286.2 (19.9) 289.1 (22.8)	529.6 (57.2) 531.4 (36.9) 533.2 (5.9)	641.4 (39.6) 642.8 (45.1) 644.5 (15.3)	1.14	0.65	239	309	442
10.0	284.7 (37.9) 285.8 (24.0) 288.7 (38.1)	529.3 (53.5) 531.3 (41.1) 532.8 (5.4)	640.8 (36.8) 642.3 (51.4) 644.7 (11.8)	1.40	0.77	235	304	427

[a] Peak percentages of the components are in parenthesis.

Please cite this article in press as: Liu, G., et al. Effects of cerium incorporation on the catalytic oxidation of benzene over flame-made perovskite $La_{1-x}Ce_xMnO_3$ catalysts. *Particuology* (2014), http://dx.doi.org/10.1016/j.partic.2014.07.001

10.0%). Similar results have been reported for Ce-doped $LaMnO_3$ (Zhang-Steenwinkel et al., 2002). The small amount of carbonate species appearing at 533.4 eV may result from the La and Ce-based perovskite, since these basic materials are easily carbonated in air (Zhang-Steenwinkel et al., 2002). In Fig. S2, the C 1s peak can be broken down into three components: hydrocarbons (284.8 eV), C—O or C=O bonds (286.2 eV), and surface carbonate species (289.2 eV) (Zhang-Steenwinkel et al., 2002).

The XPS spectra of La and Ce are presented in Figs. S3 and S4. The main peak at 833.6 eV obtained from the $La_{1-x}Ce_xMnO_3$ catalysts is generally attributed to La^{3+} in the perovskite structure. The absence of a peak at 834.7 eV demonstrates that no La_2O_3 phase is present. This result is in agreement with the XRD data showing a homogenous perovskite phase with small amounts of non-stoichiometric MnO_x species. From Fig. S4, it is obvious that a mixture of Ce^{3+} and Ce^{4+} is present at high levels of substitution (x = 5.0%, 7.5%, and 10.0%), since the characteristic peaks corresponding to Ce^{3+} and Ce^{4+} can be observed (Romeo, Bak, El Fallah, Le Normand, & Hilaire, 1993; Sohal et al., 2010). According to Zhang-Steenwinkel et al. (2002), Ce^{3+} species are dominant in a La–Mn perovskite substituted by Ce when the degree of substitution, x, is less than 10%. Similar conclusions were also derived by de Lima et al. (2012), who found that a higher fraction of Ce^{3+} ions was present in a $La_{1-x}Ce_xNiO_3$ perovskite in which x was 5.0%. These data therefore indicate that cerium was indeed incorporated into the perovskite structure. In the case of a $La_{1-x}Ce_xCoO_3$ perovskite (Ghasdi, Alamdari, Royer, & Adnot, 2011), the concentration limit for the presence of Ce^{4+} species was reported to lie between 5% and 10%. It can thus be assumed that both Ce^{3+} and Ce^{4+} species were present in the perovskite structures according to the literature reports noted above. The effect of partial substitution of La^{3+} by trivalent Ce^{3+} on the perovskite structure is negligible because of the very close match between their ionic radii (La^{3+}: 1.17 Å, Ce^{3+}: 1.15 Å) (de Lima et al., 2012). In addition, the substitution of trivalent La^{3+} by trivalent Ce^{3+} results in electronic homogeneity in the perovskite structure. By the same reasoning, the substitution of A-site La^{3+} by tetravalent Ce^{4+} ions should lead to a modified electronic effect. It is generally accepted that, concurrent with substitution by high valency ions at the A-sites of perovskite structures, the B-site ions undergo reduction to low valency states to maintain charge neutrality, and vice versa (Chen et al., 2013; de Lima et al., 2012). For the $La_{1-x}Ce_xCoO_3$ perovskites, the partial substitution of La^{3+} by Ce^{4+} results in the conversion of Co^{3+} to Co^{2+} (Ghasdi et al., 2011). Ponce et al. (2000) reported that charge compensation was achieved by oxidation of Mn^{3+} to Mn^{4+} with increasing values of x in $La_{1-x}Sr_xMnO_{3+\delta}$ samples, while Kucharczyk and Tylus (2008) found that when La^{3+} ions in $LaMnO_3$ were substituted by Ag^+ ions, two Mn^{3+} ions had to be oxidized to Mn^{4+} for every Ag^+ ion substituted. It is thus reasonable to conclude that the partial substitution of La^{3+} by Ce^{4+} may result in the conversion of Mn^{4+} to Mn^{3+} at the B-sites. Although this suggests that the surface Mn^{4+}/Mn^{3+} ratio will decrease with increasing Ce^{4+} concentrations, the opposite trend is observed in Fig. 6, in which the surface Mn^{4+}/Mn^{3+} ratio increases with the addition of Ce. In general, the incorporation of Ce into the perovskite lattice leads to increased surface Mn^{4+}/Mn^{3+} ratios, whereas the requirement for charge neutrality in the perovskite induces the reverse effect. A similar phenomenon was also observed in Kucharczyk's study (2008), in which La^{3+} was substituted by Ag^+ in $LaMnO_3$, resulting in increased Mn^{4+}/Mn^{3+} ratios due to charge neutralization. In Kucharczyk's work, two Mn^{3+} ions had to be oxidized to Mn^{4+} for every Ag^+ ion substitution, although in the case of fresh $La_{0.7}Ag_{0.3}MnO_3$, $La_{0.8}Ag_{0.2}MnO_3$, and $LaMnO_3$ catalysts, the Mn^{4+}/Mn^{3+} ratio was 1.50, 1.55, and 1.60, suggesting that the Mn^{4+}/Mn^{3+} ratio decreased with increases in the degree of Ag^+ substitution. Thus the opposite of the expected effect was observed, which is not explained by the authors. One possible explanation for the ratio increase is that the modification of the oxidation state of Mn by Ce incorporation may be accompanied by the formation of a non-stoichiometric compound. The saturation point for Ce-doping has been variously reported in other studies to be between 5 and 10 at% (Ghasdi et al., 2011). Previous XRD analyses have also suggested the possible formation of Ce—Mn—O compounds on the perovskite surface. Thus, the increased Mn^{4+}/Mn^{3+} ratio might be attributed to the formation of a non-stoichiometric Ce—Mn—O compound on the perovskite surface.

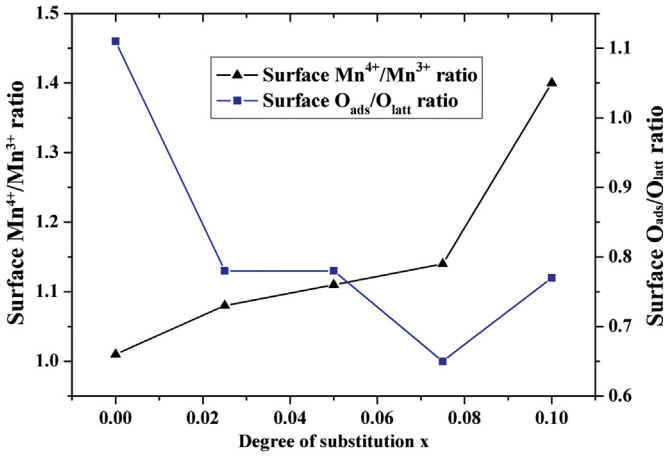

Fig. 6. Surface Mn^{4+}/Mn^{3+} and O_{ads}/O_{latt} ratios from XPS data as functions of the degree of cerium substitution.

In contrast, the decrease in the surface O_{ads}/O_{latt} ratio with increasing Ce concentration (x = 0–7.5 at%) observed in Fig. 6 may be evidence for the balancing of charge neutrality. In addition, as noted, the saturation point for Ce-doping was reported to be between 5 and 10 at% (Ghasdi et al., 2011). Thus, at the 10 at% Ce level applied in this study, the increase of O_{ads}/O_{latt} on the perovskite surface may be attributed to presence of non-stoichiometric compounds.

Reducibility and catalytic activity for benzene oxidation

The temperature-programmed reduction profiles of the $La_{1-x}Ce_xMnO_3$ catalysts were obtained to assess the presence of reducible oxygen species. Fig. 7 shows two broad reduction zones: 325–580 °C and 750–850 °C. The peak at 750–850 °C can be clearly seen, although the peak is partly cut off because of the temperature limitations of the H_2-TPR system. The reduction profiles of the $La_{1-x}Ce_xMnO_3$ catalysts in the 325–580 °C zone exhibit a broad peak, which can be broken down into two components. The first component, located at low temperatures, can be assigned to the elimination of the excess oxygen accommodated within the lattice of the perovskite structure (Ponce et al., 2000; Zhang-Steenwinkel et al., 2002). The second component is due to the reduction of Mn^{4+} as compensation for the cation vacancy caused by Ce incorporation, which is also indicated by the XPS analysis. Compared with the pure $LaMnO_3$, the initial reduction temperatures of the $La_{1-x}Ce_xMnO_3$ materials (x = 2.5%, 5.0%, 7.5%, and 10.0%) shift to lower temperatures with increasing Ce concentrations, indicating that the reduction of $La_{1-x}Ce_xMnO_3$ ($x \neq 0$) becomes much easier. The second peak, located at high temperatures, behaves similarly to the intense peak present at 325–580 °C, indicating that the reduction is a multiple-step process. Compared with the data for pure $LaMnO_3$, the 750–850 °C peaks of the Ce-treated materials also show a slight shift to lower temperatures, suggesting that the

Please cite this article in press as: Liu, G., et al. Effects of cerium incorporation on the catalytic oxidation of benzene over flame-made perovskite $La_{1-x}Ce_xMnO_3$ catalysts. *Particuology* (2014), http://dx.doi.org/10.1016/j.partic.2014.07.001

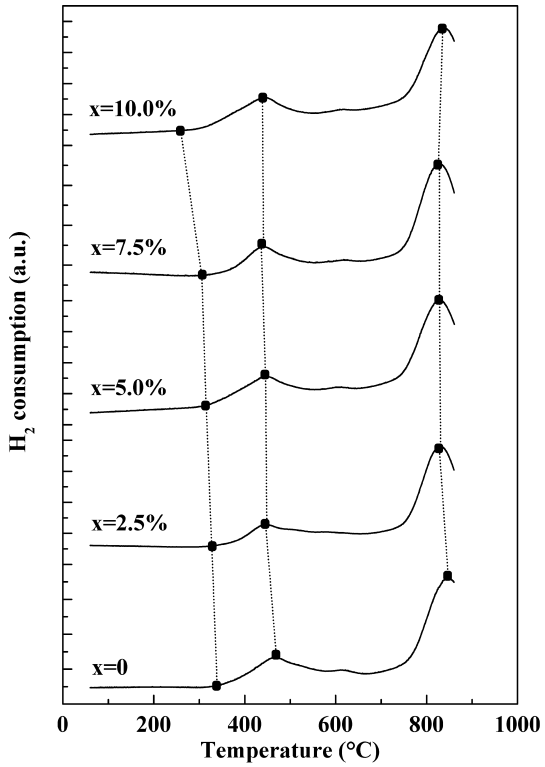

Fig. 7. H_2-TPR profiles of $La_{1-x}Ce_xMnO_3$ catalysts with varying cerium concentrations.

incorporation of Ce has a significant effect on the reducible properties of the perovskites. The second reduction peak is assigned to the reduction of Mn^{3+} to Mn^{2+}, a process that destroys the perovskite structure, as reported in previous studies (Ponce et al., 2000; Zhang-Steenwinkel et al., 2002).

The catalytic activity during benzene oxidation over the $La_{1-x}Ce_xMnO_3$ catalyst series was studied over a wide temperature range (100–450 °C). The catalytic performance, expressed as benzene conversion, is given in Fig. 8 as a function of the reaction temperature. $LaMnO_3$ exhibited moderate catalytic activity, with T_{90} located around 450 °C. In comparison, pure CeO_2 showed low activity, as seen in the inset, providing benzene conversion

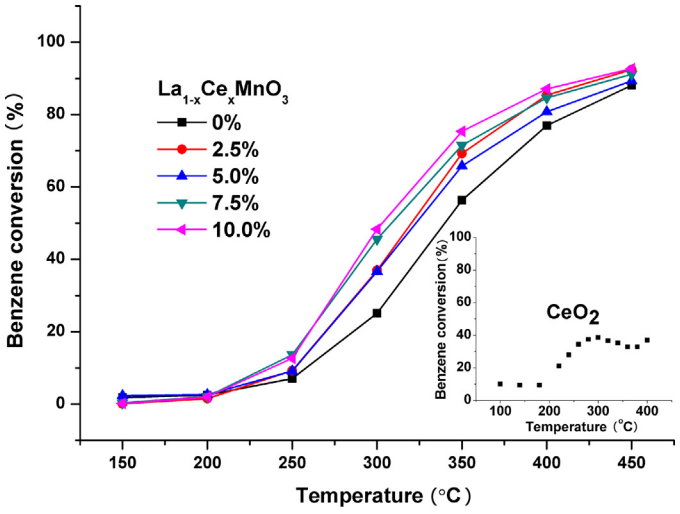

Fig. 8. Benzene conversion over $La_{1-x}Ce_xMnO_3$ catalysts as a function of temperature. Conditions: 1000 ppm benzene, 20 vol% O_2, balance N_2, 60,000 mL/(g h) WHSV.

below 40%, even at 450 °C. With increases in the Ce concentration, the benzene conversion increased by a maximum 20% with the $La_{0.900}Ce_{0.100}MnO_3$ catalyst. The temperature dependence of benzene conversion over the $La_{1-x}Ce_xMnO_3$ catalysts was also related to Ce concentration. It is evident that the $La_{1-x}Ce_xMnO_3$ catalysts outperformed the pure $LaMnO_3$ catalyst, which did not contain Ce. This result suggests that the addition of Ce into the perovskite had a positive effect on the activity for benzene catalytic oxidation. It should be noted that the benzene was completely oxidized to H_2O and CO_2 over the $La_{1-x}Ce_xMnO_3$ catalysts, and that no by-products were detected during the oxidation reaction. The temperatures corresponding to 10%, 50%, and 90% benzene conversion (T_{10}, T_{50}, and T_{90}) over the $La_{1-x}Ce_xMnO_3$ catalysts are provided in Table 2 and these materials may be listed in decreasing order of catalytic activity judging from the benzene conversion as: $La_{0.900}Ce_{0.100}MnO_3 > La_{0.925}Ce_{0.075}MnO_3 > La_{0.950}Ce_{0.050}MnO_3 > La_{0.975}Ce_{0.025}MnO_3 > LaMnO_3$.

The activity of the $La_{1-x}Mn_xO_3$ perovskite catalysts during catalytic oxidation reactions has been found to depend on two main factors: the SSA of the perovskite and the surface composition of the catalyst. According to literature reports, the SSA of perovskites largely depends on the preparation method. Kucharczyk and Tylus (2008) reported partial substitution of La by Ag in $LaMnO_3$ perovskite and found that the SSA of the material increased after Ag incorporation. In the present catalysts, however, Ce incorporation was not observed to change the SSA value dramatically. The effect of SSA on catalytic activity therefore appears negligible since all catalysts produced in this work had approximately equal SSA values within the measurement uncertainty. The substituted perovskite catalysts prepared by flame spray pyrolysis, however, display several differences in their structures and catalytic activity. In perovskite oxides, substitution of the trivalent A-site ions (La^{3+}) by a metal ion with a different valency is accompanied by a change in the oxidation state of B-site ions to maintain charge neutrality, which subsequently changes the catalytic activity. It has been reported that this charge compensation is achieved by oxidation of Mn^{3+} to Mn^{4+} as the x value in $La_{1-x}Sr_xMnO_{3+\delta}$ increases, such that the Mn^{4+}/Mn^{3+} ratio increases (Ponce et al., 2000). Theoretically, the substitution of Ce^{4+} could also lead to a decrease in the Mn^{4+}/Mn^{3+} ratio as a means of neutralizing the excess charge. In Fig. 6, an increase in the surface Mn^{4+}/Mn^{3+} ratio is observed after Ce incorporation, which is accompanied by a decrease in the surface O_{ads}/O_{latt} ratio. Modification of the oxidation state of B-site Mn ions by incorporation of A-site ions is accompanied by the formation of non-stoichiometric oxides. Specifically, this suggests that excess oxygen is accommodated within the lattice of the perovskite structure (Ponce et al., 2000; Vogel, Johnson, & Gallagher, 1977), as indicated by the initial peak observed in the range of 325–580 °C in the H_2-TPR data. These H_2-TPR results suggest that differences in oxidation state lead to variations in the reducibility of the catalyst, since both the Mn^{4+} to Mn^{3+} and Mn^{3+} to Mn^{2+} reduction peaks were shifted to slightly lower temperatures, suggesting enhanced reducibility. Meanwhile, the blue shift of the initial reduction temperature assigned to oxygen accommodated within the lattice of the perovskite structure also indicated that the Ce substitution facilitated the oxygen transfer and thus enhanced the catalytic activity.

The mechanism of the catalytic combustion of VOCs over reducible metal oxides is reported to follow the Mars and van Krevelen mechanism (Liu, Yue, et al., 2013; Liu, Dai, et al., 2013). The key steps involve the supply of active oxygen species by the reducible metal oxide and the oxidation of this species by gas phase oxygen (Liu, Dai, et al., 2013). Fig. 9 shows the correlation between the surface Mn^{4+}/Mn^{3+} ratio and the catalytic activity (T_{50}). As can be seen, the surface Mn^{4+} concentration exhibits a reasonable

Please cite this article in press as: Liu, G., et al. Effects of cerium incorporation on the catalytic oxidation of benzene over flame-made perovskite $La_{1-x}Ce_xMnO_3$ catalysts. *Particuology* (2014), http://dx.doi.org/10.1016/j.partic.2014.07.001

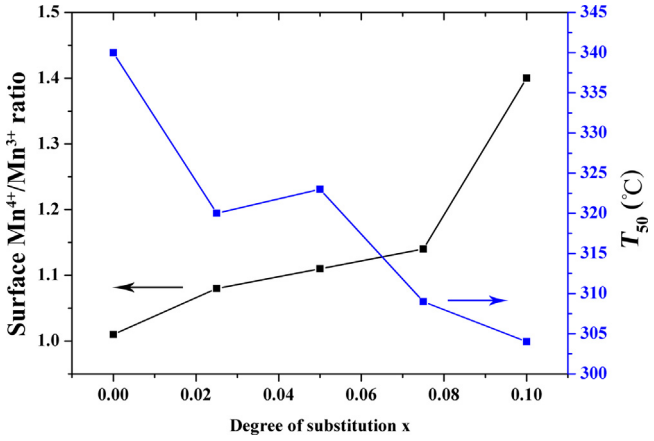

Fig. 9. The relationships between surface Mn^{4+}/Mn^{3+} ratio and T_{50} with the perovskite degree of cerium substitution.

correlation with the benzene oxidation activity. Higher Mn oxidation states could promote the redox properties of the material (Chen et al., 2013) and so the shift of B-site metal ions between Mn^{4+} and Mn^{3+} due to cerium incorporation is believed to play a role in the benzene catalytic oxidation reaction, which represents a redox process over metal oxide catalysts (Liu, Yue, et al., 2013).

Conclusion

$La_{1-x}Ce_xMnO_3$ (x = 1–10%) perovskites with a single crystal structure were prepared by flame spray pyrolysis and the $La_{0.900}Ce_{0.100}MnO_3$ catalyst exhibited the best catalytic activity for benzene oxidation. Ce^{4+} substitution had a negligible effect on the SSA of the resulting $La_{1-x}Ce_xMnO_3$ perovskites and hence the SSA has less impact on the catalytic activity for benzene oxidation. The substitution of La^{3+} by Ce^{4+} resulted in an increase in the surface Mn^{4+}/Mn^{3+} ratio and a decrease in the surface O_{ads}/O_{latt} ratio due to charge neutralization. These trends in the Mn^{4+}/Mn^{3+} and O_{ads}/O_{latt} ratios exhibit good correlation with the catalytic activity during benzene oxidation, indicating that the Ce^{4+}-induced modification of the Mn^{4+}/Mn^{3+} ratio and the oxygen species was accompanied by enhanced catalytic activity.

Acknowledgments

The authors gratefully acknowledge the financial support of the National High Technology Research and Development Program of China (Grant Nos. 2012AA062702 and 2010AA064903), the Strategic Priority Research Program of the Chinese Academy of Sciences (Grant No. XDB05050300), the National Natural Science Foundation of China (No. 21306199), the Instrument Developing Project of the Chinese Academy of Sciences (Grant No. YZ200722) and the 12th Five-years National Key Technology R&D Program (Grant Nos. 2012BAJ02B03 and 2012BAJ02B07).

Appendix A. Supplementary data

Supplementary material related to this article can be found, in the online version, at http://dx.doi.org/10.1016/j.partic.2014.07.001.

References

Alifanti, M., Kirchnerova, J., & Delmon, B. (2003). Effect of substitution by cerium on the activity of $LaMnO_3$ perovskite in methane combustion. *Applied Catalysis A: General*, *245*, 231–243.

Asamoto, M., & Yahiro, H. (2009). Catalytic property of perovskite-type oxide prepared by thermal decomposition of heteronuclear complex. *Catalysis Surveys from Asia*, *13*, 221–228.

Azurdia, J. A., Marchal, J., Shea, P., Sun, H. P., Pan, X. Q., & Laine, R. M. (2006). Liquid-feed flame spray pyrolysis as a method of producing mixed-metal oxide nanopowders of potential interest as catalytic materials. Nanopowders along the NiO–Al_2O_3 tie line including $(NiO)_{0.22}(Al_2O_3)_{0.78}$, a new inverse spinel composition. *Chemistry of Materials*, *18*, 731–739.

Blasin-Aube, V., Belkouch, J., & Monceaux, L. (2003). General study of catalytic oxidation of various VOCs over $La_{0.8}Sr_{0.2}MnO_{3+x}$ perovskite catalyst-influence of mixture. *Applied Catalysis B: Environmental*, *43*, 175–186.

Buchneva, O., Rossetti, I., Biffi, C., Allieta, M., Kryukov, A., & Lebedeva, N. (2009). La–Ag–Co perovskites for the catalytic flameless combustion of methane. *Applied Catalysis A: General*, *370*, 24–33.

Campagnoli, E., Tavares, A., Fabbrini, L., Rossetti, I., Dubitsky, Y. A., Zaopo, A., et al. (2005). Effect of preparation method on activity and stability of $LaMnO_3$ and $LaCoO_3$ catalysts for the flameless combustion of methane. *Applied Catalysis B: Environmental*, *55*, 133–139.

Chen, J., Shen, M., Wang, X., Qi, G., Wang, J., & Li, W. (2013). The influence of nonstoichiometry on $LaMnO_3$ perovskite for catalytic NO oxidation. *Applied Catalysis B: Environmental*, *134–135*, 251–257.

Chiarello, G. L., Ferri, D., Grunwaldt, J. D., Forni, L., & Baiker, A. (2007). Flame-synthesized $LaCoO_3$-supported Pd: 2. Catalytic behavior in the reduction of NO by H_2 under lean conditions. *Journal of Catalysis*, *252*, 137–147.

Chiarello, G. L., Grunwaldt, J. D., Ferri, D., Krumeich, R., Oliva, C., Forni, L., et al. (2007). Flame-synthesized $LaCoO_3$-supported Pd: 1. Structure, thermal stability and reducibility. *Journal of Catalysis*, *252*, 127–136.

Chiarello, G. L., Rossetti, I., & Forni, L. (2005). Flame-spray pyrolysis preparation of perovskites for methane catalytic combustion. *Journal of Catalysis*, *236*, 251–261.

Chiarello, G. L., Rossetti, I., Lopinto, P., Migliavacca, G., & Forni, L. (2006). Preparation by flame spray pyrolysis of $ABO_{3\pm\delta}$ catalysts for the flameless combustion of methane. *Catalysis Today*, *117*, 549–553.

de Lima, S. M., da Silva, A. M., da Costa, L. O. O., Assaf, J. M., Mattos, L. V., Sarkari, R., et al. (2012). Hydrogen production through oxidative steam reforming of ethanol over Ni-based catalysts derived from $La_{1-x}Ce_xNiO_3$ perovskite-type oxides. *Applied Catalysis B: Environmental*, *121–122*, 1–9.

Ghasdi, M., Alamdari, H., Royer, S., & Adnot, A. (2011). Electrical and CO gas sensing properties of nanostructured $La_{1-x}Ce_xCoO_3$ perovskite prepared by activated reactive synthesis. *Sensors and Actuators B: Chemical*, *156*, 147–155.

Kaddouri, A., Gelin, P., & Dupont, N. (2009). Methane catalytic combustion over La–Ce–Mn–O-perovskite prepared using dielectric heating. *Catalysis Communications*, *10*, 1085–1089.

Kucharczyk, B., & Tylus, W. (2008). Partial substitution of lanthanum with silver in the $LaMnO_3$ perovskite: Effect of the modification on the activity of monolithic catalysts in the reactions of methane and carbon oxide oxidation. *Applied Catalysis A: General*, *335*, 28–36.

Li, W. B., Wang, J. X., & Gong, H. (2009). Catalytic combustion of VOCs on non-noble metal catalysts. *Catalysis Today*, *148*, 81–87.

Liu, G., Yue, R. L., Jia, Y., Ni, Y., Yang, J., Liu, H. D., et al. (2013). Catalytic oxidation of benzene over Ce–Mn oxides synthesized by flame spray pyrolysis. *Particuology*, *11*, 454–459.

Liu, Y., Dai, H., Deng, J., Zhang, L., Gao, B., Wang, Y., et al. (2013). PMMA-templating generation and high catalytic performance of chain-like ordered macroporous $LaMnO_3$ supported gold nanocatalysts for the oxidation of carbon monoxide and toluene. *Applied Catalysis B: Environmental*, *140–141*, 317–326.

Najjar, H., & Batis, H. (2010). La–Mn perovskite-type oxide prepared by combustion method: Catalytic activity in ethanol oxidation. *Applied Catalysis A: General*, *383*, 192–201.

Niu, J. R., Deng, J. G., Liu, W., Zhang, L., Wang, G. Z., Dai, H. X., et al. (2007). Nanosized perovskite-type oxides $La_{1-x}Sr_xMO_{3-\delta}$ (M = CO, Mn; x = 0, 0.4) for the catalytic removal of ethylacetate. *Catalysis Today*, *126*, 420–429.

Pecchi, G., Reyes, P., Zamora, R., Cadus, L. E., & Fierro, J. L. G. (2008). Surface properties and performance for VOCs combustion of $LaFe_{1-y}Ni_yO_3$ perovskite oxides. *Journal of Solid State Chemistry*, *181*, 905–912.

Pinsard-Gaudart, L., Rodriguez-Carvajal, J., Daoud-Aladine, A., Goncharenko, I., Medarde, M., Smith, R. L., et al. (2001). Stability of the Jahn–Teller effect and magnetic study of $LaMnO_3$ under pressure. *Physical Review B*, *64*, 064426.

Ponce, S., Peña, M. A., & Fierro, J. L. G. (2000). Surface properties and catalytic performance in methane combustion of Sr-substituted lanthanum manganites. *Applied Catalysis B: Environmental*, *24*, 193–205.

Romeo, M., Bak, K., El Fallah, J., Le Normand, F., & Hilaire, L. (1993). XPS study of the reduction of cerium dioxide. *Surface and Interface Analysis*, *20*, 508–512.

Rossetti, I., Biffi, C., & Forni, L. (2010). Oxygen non-stoichiometry in perovskitic catalysts: Impact on activity for the flameless combustion of methane. *Chemical Engineering Journal*, *162*, 768–775.

Roy, S., van Vegten, N., & Baiker, A. (2010). Single-step flame-made $Pt/MgAl_2O_4$: A NO_x storage-reduction catalyst with unprecedented dynamic behavior and high thermal stability. *Journal of Catalysis*, *271*, 125–131.

Royer, S., Alamdari, H., Duprez, D., & Kaliaguine, S. (2005). Oxygen storage capacity of $La_{(1-x)}A'_xBO_3$ perovskites (with A′ = Sr, Ce; B = Co, Mn)-relation with catalytic activity in the CH_4 oxidation reaction. *Applied Catalysis B: Environmental*, *58*, 273–288.

Sohal, R., Lupina, G., Seifarth, O., Zaumseil, P., Walczyk, C., & Schroeder, T. (2010). Improving the dielectric constant of Al_2O_3 by cerium substitution for high-k MIM applications. *Surface Science*, *604*, 276–282.

Please cite this article in press as: Liu, G., et al. Effects of cerium incorporation on the catalytic oxidation of benzene over flame-made perovskite $La_{1-x}Ce_xMnO_3$ catalysts. *Particuology* (2014), http://dx.doi.org/10.1016/j.partic.2014.07.001

Spinicci, R., Faticanti, M., Marini, P., De Rossi, S., & Porta, P. (2003). Catalytic activity of $LaMnO_3$ and $LaCoO_3$ perovskites towards VOCs combustion. *Journal of Molecular Catalysis A: Chemical*, *197*, 147–155.

Talati, M., & Jha, P. K. (2006). Structure dependent phonon properties of $LaMnO_3$. *Computational Materials Science*, *37*, 64–68.

Teoh, W. Y., Madler, L., Beydoun, D., Pratsinis, S. E., & Amal, R. (2005). Direct (one-step) synthesis of TiO_2 and Pt/TiO_2 nanoparticles for photocatalytic mineralisation of sucrose. *Chemical Engineering Science*, *60*, 5852–5861.

Teraoka, Y., Kanada, K., & Kagawa, S. (2001). Synthesis of La–K–Mn–O perovskite-type oxides and their catalytic property for simultaneous removal of NO_x and diesel soot particulates. *Applied Catalysis B: Environmental*, *34*, 73–78.

Thiebaut, B. T. B. (2011). Flame spray pyrolysis: A unique facility for the production of nanopowders. *Platinum Metals Review*, *55*, 149–151.

Vogel, E. M., Johnson, D. W., & Gallagher, P. K. (1977). Oxygen stoichiometry in $LaMn_{1-x}Cu_xO_{3+y}$ by thermogravimetry. *Journal of the American Ceramic Society*, *60*, 31–33.

Wen, Y., Zhang, C., He, H., Yu, Y., & Teraoka, Y. (2007). Catalytic oxidation of nitrogen monoxide over $La_{1-x}Ce_xCoO_3$ perovskites. *Catalysis Today*, *126*, 400–405.

Zhang-Steenwinkel, Y., Beckers, J., & Bliek, A. (2002). Surface properties and catalytic performance in CO oxidation of cerium substituted lanthanum–manganese oxides. *Applied Catalysis A: General*, *235*, 79–92.

Please cite this article in press as: Liu, G., et al. Effects of cerium incorporation on the catalytic oxidation of benzene over flame-made perovskite $La_{1-x}Ce_xMnO_3$ catalysts. *Particuology* (2014), http://dx.doi.org/10.1016/j.partic.2014.07.001